ACS Catalysis

Research Article

pubs.acs.org/acscatalysis

Computed Propagation and Termination Steps in [(Cycloocta-2,6-dien-1-yl)Rh^{III}(polymeryl)]$^+$ Catalyzed Carbene Polymerization Reactions

Annemarie J. C. Walters, Joost N.H. Reek, and Bas de Bruin*

Van 't Hoff Institute for Molecular Sciences (HIMS), Homogeneous and Supramolecular Catalysis group, Universiteit van Amsterdam (UvA), P.O. Box 94720, 1090 GS Amsterdam, The Netherlands

Supporting Information

ABSTRACT: This paper discloses the DFT-computed pathways for chain propagation, chain transfer, and chain termination during carbene polymerization catalyzed by cationic [(cycloocta-2,6-dien-1-yl)Rh^{III}(alkyl)]$^+$ species. In contrast to carbene polymerization calculated for neutral [(cod)Rh^{I}(alkyl)]$^+$ catalysts, chain propagation at the cationic [(cycloocta-2,6-dien-1-yl)Rh^{III}(alkyl)]$^+$ species is clearly competitive with β-hydride elimination, thus explaining the formation of high molecular weight polymers. Computed chain-end-controlled chain propagation reveals a clear preference for syndiotactic polymerization. Chain transfer involving alcohol-mediated protonolysis is computed to be a more favorable pathway than β-hydride elimination. These results are all in agreement with experimental observations. Chain propagation from species with a stereoerror at the α-carbon atom of the growing chain is substantially slower compared to propagation from syndiotactic species without stereoerrors, providing a possible explanation for the experimentally observed low initiation efficiencies of the Rh catalysts in carbene polymerization reactions. These new computational insights, combined with experimental results disclosed in earlier reports, largely clarify the mechanism of Rh-mediated carbene polymerization reactions.

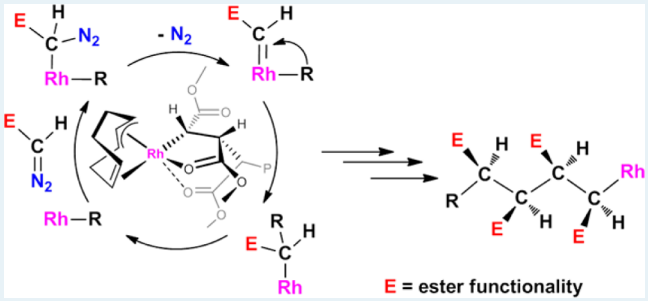

KEYWORDS: *carbene polymerization, diazo compounds, rhodium, computational studies, DFT*

1. INTRODUCTION

C1 polymerization (carbene polymerization) offers an interesting alternative synthetic approach to polymers that are currently not available via more traditional polymerization of vinyl monomers (C2 polymerization). Transition-metal-catalyzed polymerization of functionalized C1 monomers (carbene monomer precursors) is a powerful synthetic method to obtain functionalized polymers with a large structural diversity.[1−28] Related synthetic methods that build up a polymer chain from C1 monomers are the boron-mediated polyhomologation techniques developed by Shea and co-workers, using sulfur-ylides as monomers, which make it possible to prepare polymers with a precise control over the nature of the end-group functionalities.[29−36] Sulfoxonium ylides are also suitable carbene monomer precursors in transition-metal-catalyzed C1 polymerization reactions.[37]

The synthesis of stereoregular, high molecular weight, densely functionalized sp^3-carbon-chain polymers that contain a polar substituent at every carbon of the polymer backbone is currently restricted to the Rh-mediated carbene polymerization techniques developed in our group (C1 polymerization).[1−20] These polymerization reactions involve a chain growth process in which the polymer chain is built up by a sequence of migratory insertion steps involving carbene units generated at chain-bearing rhodium complexes (Scheme 1). Typically, syndiotactic polymers are produced, which in the case of C1 polymerization reactions means that the substituents all point to the same side of the polymer when the chain is projected in a regular zigzag conformation.[38]

Although the basic carbene-insertion mechanism shown in Scheme 1 was quickly established for the Rh-mediated carbene polymerization, several details of the polymerization mechanism have remained unclear for quite a while. In particular, it proved quite challenging to determine the structure of the active Rh species as well as establishing certain details about the initiation, termination, and chain-transfer mechanisms. However, recent mechanistic investigations have shed more light on these matters.[20] On the basis of a combination of ESI-MS spectrometry, catalytic reactions, and kinetic studies using discrete oxygenated Rh(cod) species, important new details were provided explaining several crucial steps of the polymerization reaction, all based on experimental observations: (a) Initiation of the reaction involves participation of water or a nucleophilic alcohol moiety. (b) The termination process

Received: February 6, 2014
Revised: March 21, 2014
Published: March 24, 2014

   dx.doi.org/10.1021/cs500160c | ACS Catal. 2014, 4, 1376−1389

Scheme 1[a]

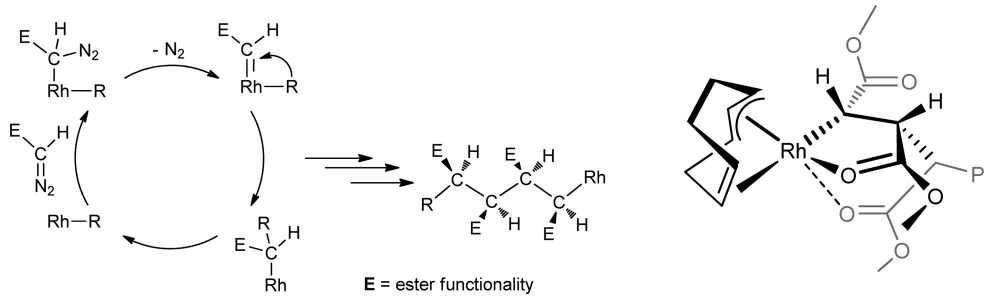

[a]Left: Rh-mediated carbene polymerization leading to fully functionalized, high molecular weight, and syndiotactic carbon-chain polymers. Right: cationic [(cycloocta-2,6-dien-1-yl)Rh^{III}(polymeryl)]$^+$ complexes experimentally demonstrated to be the active species responsible for polymer formation[20].

involves water or alcohol present in the reaction medium, leading to protonation of the Rh-alkyl chain. (c) Cationic [(allyl)Rh^{III}(polymeryl)]$^+$ species (Scheme 1) mediate the reaction rather than neutral [(diene)Rh^{I}(polymeryl)] species. (d) These active species are most efficiently (but not exclusively) generated by oxygenation of the metal−olefin precursors.[39−49]

Despite the fact that these data added important pieces to the puzzle, several details about the propagation, chain-transfer, and termination steps of carbene polymerization reaction using [(allyl)Rh^{III}(polymeryl)]$^+$ species remained (thus far) rather unclear. In particular, the following main questions remain to be answered:

(1) Why does the polymerization reaction proceed with a high syndio-specificity?
(2) Why are high molecular weight polymers obtained?
(3) Why are saturated polymers formed rather than unsaturated ones?
(4) What is the reason for the low initiation efficiency of the catalyst (<10%)?

Some of the above questions were previously explored assuming polymer formation at neutral [(diene)-Rh^{I}(polymeryl)] species.[6,10] On the basis of the available experimental data, assuming polymerization activity for neutral [(diene)Rh^{I}(polymeryl)] species seemed most plausible (although some doubts about the rhodium oxidation state was noted before[50,51]). However, this assumption was contradicted by several experimental observations in follow-up studies.[12] Most importantly, the experimentally observed formation of long polymers from neutral [(diene)-Rh^{I}(polymeryl)] species could not be explained, neither experimentally nor computationally.[10−12] Hence, new computational studies are in place, building on the mechanistic information disclosed in ref 20 showing that the active polymer-growing species are cationic [(cycloocta-2,6-dien-1-yl)Rh^{III}(polymeryl)]$^+$ complexes (see Scheme 1) rather than neutral [(diene)Rh^{I}(polymeryl)] species. In this paper, we describe the results of a computational study aimed at answering the above questions and providing detailed mechanistic information about the chain-propagation, chain-transfer, and chain-termination steps occurring during carbene polymerization reactions catalyzed by [(cycloocta-2,6-dien-1-yl)Rh^{III}(polymeryl)]$^+$ species.

2. RESULTS AND DISCUSSION

2.1. Applied DFT Methods. In order to gain a better insight into the propagation of the polymerization, we performed DFT calculations to estimate the energies and the differences in energies of the different steps in the propagation. We used the hybrid b3-lyp functional as defined in the Turbomole libraries and the large Ahlrichs def2-TZVP basis set, which is a commonly used combination with proven accuracy for DFT calculations on rhodium complexes. We optimized all geometries using Grimme's D3 dispersion (disp3) corrections to the DFT calculations in order to account for van der Waals interactions between the ligand/substrate fragments. Without these corrections, we obtained unrealistically high energies for all steps involving substrate binding and activation. The primary effect of the dispersion corrections is its effect on the binding energies of the diazo compound as well as its influence on the position of the oxygen atoms of the ester moieties, making the units more compact. The large number of oxygen atoms present in the molecule led to quite large effects of the dispersion corrections on the energies obtained (initial calculations showed energy difference between species **A**, **B**, and **TS1** without dispersion correction of 15.5 and 28.6 kcal mol^{-1} and with dispersion correction, respectively, of 1.1 and 11.7 kcal mol^{-1}). To confirm that these effects are indeed related to dispersion forces rather than unforeseen effects of the (partially empirical) disp3 correction terms, the calculated energy barrier for **TS1** (versus **A** + MDA; see Figure 2) with disp3 dispersion corrections were compared to the calculated energy barrier for **TS1** with correlated Møller−Plesset (MP2) perturbation theory calculations. The relative values of **TS1** are nearly the same (11.0 kcal mol^{-1} with MP2 -def2-TZVP versus 10.9 kcal mol^{-1} for the energies with b3-lyp-def2-TZVP-disp3). Therefore we performed all further calculations with DFT-D3 using the b3-lyp functional and the def2-TZVP basis set and Grimme's dispersion corrections (version D3, implemented in Turbomole as "disp3") rather than expensive (time-consuming) MP2 calculations.

2.2. Identifying the Most Stable Start Geometries. The experimental data disclosed in ref 20 indicated that the active species for the polymerization is a cationic [(cycloocta-2,6-dien-1-yl)Rh^{III}(polymery)]$^+$ species. For the DFT calculations, this species was simplified to a [(cycloocta-2,6-dien-1-yl)Rh^{III}({CH-(COOMe)}$_3$CH$_3$)]$^+$ species containing a short, three-carbon syndiotactic chain to reduce the calculation times. We argued that no less than three consecutive carbene insertion steps were needed to model the growing polymer chain in a realistic manner. Two of the ester carbonyl moieties tend to coordinate

dx.doi.org/10.1021/cs500160c | ACS Catal. 2014, 4, 1376−1389

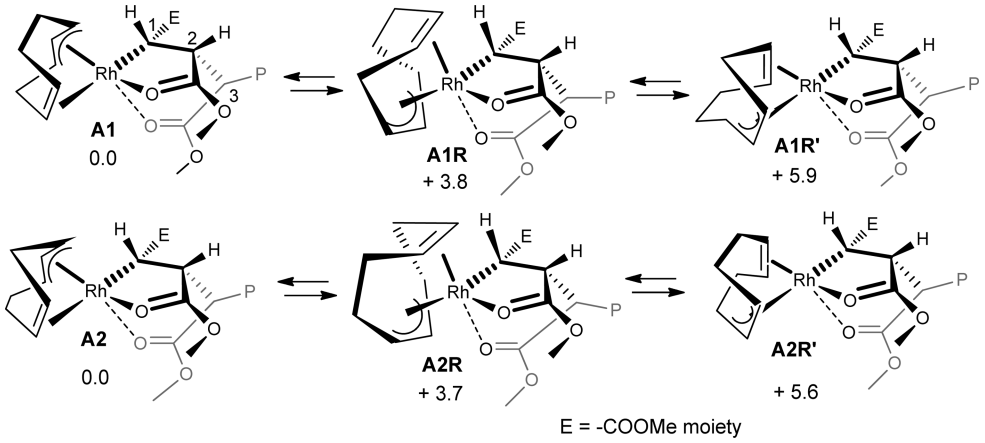

Figure 1. Various geometrical and conformational isomers of species **A**. Diastereomers **A1** and **A2** (alkyl trans to the olefinic double bond of the cycloocta-2,6-dien-1-yl ligand) and their higher energy rotameric forms **A1R, A1R′**, **A2R**, and **A2R′** (alkyl trans to the allyl moiety of the cycloocta-2,6-dien-1-yl ligand). Relative free energies (ΔG°_{298K}) in kcal mol^{-1} (b3-lyp, def2-TZVP, corrected for van der Waals interactions (disp3)).

to the Rh^{III} center. Furthermore, a smaller model of EDA was used: methyl diazoacetate (MDA). All calculated pathways start from the $[(\text{cycloocta-2,6-dien-1-yl})Rh^{III}(\{CH(COOMe)\}_3CH_3)]^+$ species (species, **A**). Before calculating the energetic pathway of the propagation of the polymerization, we optimized different geometrical isomers of species **A** to find out which geometry is lowest in energy. The (cycloocta-2,6-dien-1-yl) ligand is chiral, as is the syndiotactic growing chain, which leads to diastereomeric combinations. Furthermore, several different geometrical isomers are possible as a result of different mutual trans arrangements of the alkyl, carbonyl, alkene, and allyl moieties. Moreover, we had to explore several conformational positions of the ester moieties of the syndiotactic growing chain, which can rotate in several different orientations. The lowest energy configurations of all species investigated are shown in Figure 1. It is worth noting that two carbonyl oxygen atoms of the growing chain coordinate to the Rh^{III} center in all of the geometrical isomers shown. Coordination of only one carbonyl oxygen atom or ester methoxy oxygen atom is also possible, but these structures are substantially higher in energy (~13 kcal mol^{-1}) and were therefore not considered in subsequent calculations.

All of the calculated structures **A** have a five-membered chelate ring in the equatorial plane of the overall distorted octahedral geometries around rhodium. This ring consists of the Rh center, the carbon atoms of the last two inserted ester units, and the β-carbonyl fragment. The carbonyl oxygen of the third-to-last inserted ester unit also coordinates to Rh^{III}, further stabilizing the complex (see geometry **A1**, for example, in Figure 1). The alkyl carbon of the growing polymer can be coordinated to the Rh(cycloocta-2,6-dien-1-yl) moiety either trans to the olefinic double bond of the cycloocta-2,6-dien-1-yl ligand (isomers **A1** and **A2**) or trans to the allylic unit (isomers **A1R, A1R′**, **A2R**, and **A2R′**). The isomers **A1** and **A2** are about 3.7 kcal mol^{-1} more stable than isomers **A1R** and **A2R** due to the strong trans influence of the negatively charged alkyl moiety, favoring its trans position with respect to the olefinic moiety rather than the allylic moiety of the cycloocta-2,6-dien-1-yl ligand. The rotamers **A1R′** and **A2R′** also have an unfavorable trans orientation of the alkyl and allyl moieties. Placing the olefinic double bond of the cycloocta-2,6-dien-1-yl ligand trans to the carbonyl donor of the six-membered chelate ring of the growing polymer chain (**A1R** and **A2R**) proves to be more favorable than placing it trans to the carbonyl donor of the five-membered chelate ring (**A1R′** and **A2R′**), presumably for steric reasons.

Whereas species **A1** and **A2** are diastereomers of each other, species **A1R** and **A1R′** are rotamers of diastereomer **A1**, in which the chiral cycloocta-2,6-dien-1-yl ligand has simply rotated in a different orientation with respect to the alkyl and carbonyl donors of the syndiotactic growing chain. Similarly, **A2R** and **A2R′** are rotamers of diastereomer **A2.** The diastereomers **A1** and **A2** (like the diastereomers **A1R** versus **A2R** and **A1R′** versus **A2R′**) differ only in the arrangement of the $-CH_2-$ and the $-CH_2-CH_2-$ fragments of the chiral cycloocta-2,6-dien-1-yl ligand. This has only a marginal effect on the relative energy of these species (<0.3 kcal mol^{-1}). However, in the isomers **A1** and **A2R**, the substrate binding site (i.e., the position trans to the coordinated ester carbonyl moiety bound to carbon 3, see Figure 1) is sterically somewhat less hindered than in the isomers **A2** and **A1R** (see section 2.3). This affects the MDA substrate binding event to some extent, which is essential for chain growth. Of course, the diastereomers **A1** and **A2** (and their rotamers) exist in two enantiomeric forms. However, enantiomers show identical catalytic polymerization reactivity,[52] and hence, it suffices to focus on only one enantiomer.

2.3. MDA Substrate Binding to Species A. To engage chain growth via a carbene polymerization mechanism, the diazo substrate (MDA) needs to coordinate to the Rh^{III} center in a cis position to the syndiotactic growing chain. The Rh centers of the various isomers of species **A**, however, are coordinatively and electronically saturated (18 valence electron, 6-coordinated species). Hence, MDA must substitute one of the coordinated carbonyl moieties attached to the syndiotactic growing chain to allow the coordination of a carbene moiety. The weaker bound ester attached to carbon 3 (numbering shown in Figure 1) is more likely to be substituted by MDA than the stronger bound ester moiety attached to carbon 2 (for the large Rh metal center, five-membered chelate rings are typically more stable than six-membered chelate rings).[53] Ligand substitution processes at Rh^{III} (like most other d^6 octahedral transition metal complexes having a filled t_{2g} d-orbital configuration) commonly proceed via a dissociatively activated interchange mechanism (I_d substitution mechanism).[52,54] In this process, binding of the incoming ligand

dx.doi.org/10.1021/cs500160c | ACS Catal. 2014, 4, 1376−1389

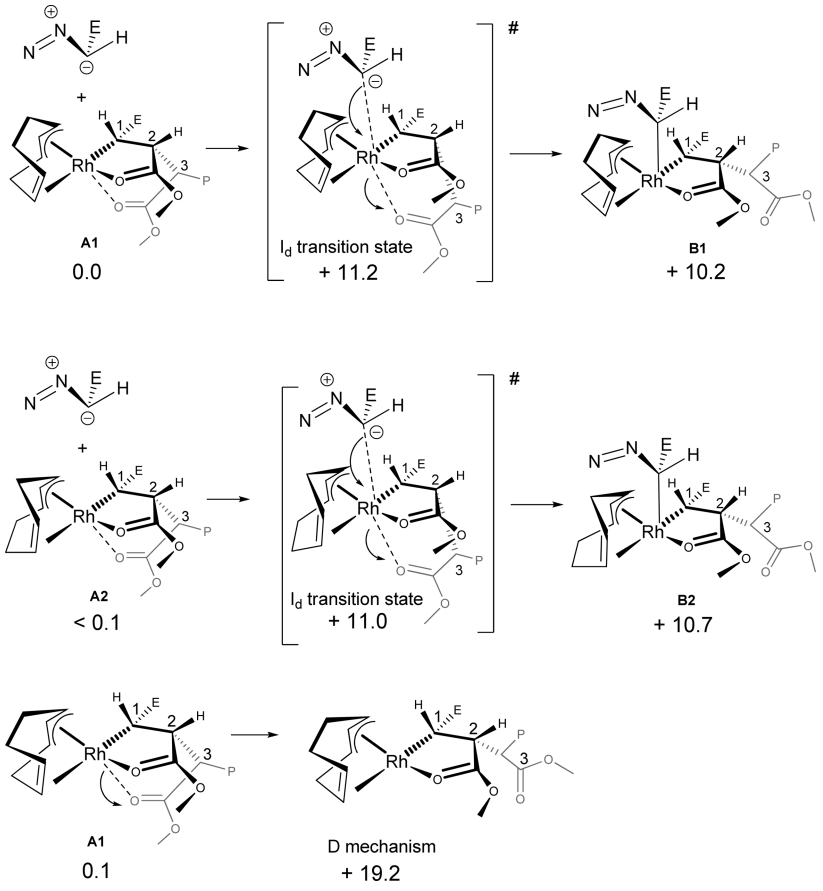

Figure 2. Interchange (I_d) mechanism for MDA binding for species **A1** and **A2**. Bottom picture shows the energy for dissociative mechanism in kcal/mol.

and dissociation of the leaving ligand proceed in a concerted manner (despite the fact that in the transition state of the I_d substitution process bond formation with the incoming ligand/substrate somewhat lags behind the bond dissociation of the leaving ligand). A similar process should occur in the formation of the MDA adducts **B** upon reaction of species **A** with the diazo substrate. As such, simultaneously with elongation of Rh−O bond upon dissociation of the carbonyl moiety attached to carbon 3 (six-membered chelate ring), the incoming MDA substrate must approach the metal center at the least hindered site, which is the coordination site trans to the leaving carbonyl moiety (see Figure 2). An alternative sequential process in which the carbonyl group of the six-memberered ring chelate attached to carbon 3 first dissociates from **A1** or **A2**, followed by MDA binding to this same position (dissociative, D mechanism) is very unlikely according to our DFT calculations. Unsupported dissociation of this carbonyl group at species **A1** has a prohibitively high energy (19.0 kcal mol^{-1} relative to **A1**).[55]

The computed I_d mechanism shown in Figure 2 is much more favorable, allowing fast ligand substitution at rhodium(III) species **A1** or **A2** to form the required MDA adducts **B1** and **B2**, respectively. Facile MDA binding is essential in the sequence of reaction steps leading to carbene polymerization.

Because the carbene polymerization reaction produces syndiotactic polymer,[1−20] the subsequent carbene insertion steps lead to alternating R- and S-configured α-carbon atoms (carbon 1 in Figure 2) of the syndiotactic growing chain. Hence, both diastereomers **A1** and **A2** must be involved in the polymerization mechanism of the same polymeric chain. The higher energy rotamers **A1R** and **A2R** may also play a role in the propagation mechanism, as they should be formed as intermediates directly after migratory carbene insertion at **A1** and **A2**, respectively. However, it makes sense to assume that propagation proceeds from the lowest energy species **A1** and **A2** and that the higher energy rotamers **A1R**, **A1R′**, **A2R**, and **A2R′** easily rearrange to the lowest energy species (**A1** and **A2**). Although we did not directly evaluate the ligand rotation barriers computationally,[56] the fact that the allyl moiety of the cycloocta-2,6-dien-1-yl ligand easily rotates away to make room for an incoming MDA substrate (see Figure 2 and discussion underneath) implies that these barriers should be low (especially compared to the rate-limiting substrate activation steps, vide infra). For simplicity, we therefore concentrate on chain propagation from the lowest energy rotameric forms of diastereomers **A1** and **A2**.

Binding of MDA to **A1** to form adduct **B1** is endergonic by 10.2 kcal mol^{-1}, and MDA binding to **A2** to form adduct **B2** is endergonic by 10.7 kcal mol^{-1}. This is a marginal energy difference and should not significantly affect chain propagation from either **A1** or **A2** (as is required in a syndiotactic polymerization mechanism).

Below, we focus on the DFT-calculated propagation and termination mechanisms (sections 2.4 and 2.5). Chain propagation and β-hydride elimination were explored from both diastereomers **A1** and **A2** (in their lowest energy rotameric forms). To simplify the analysis and to minimize computational time, we restricted our calculations of the

dx.doi.org/10.1021/cs500160c | ACS Catal. 2014, 4, 1376−1389

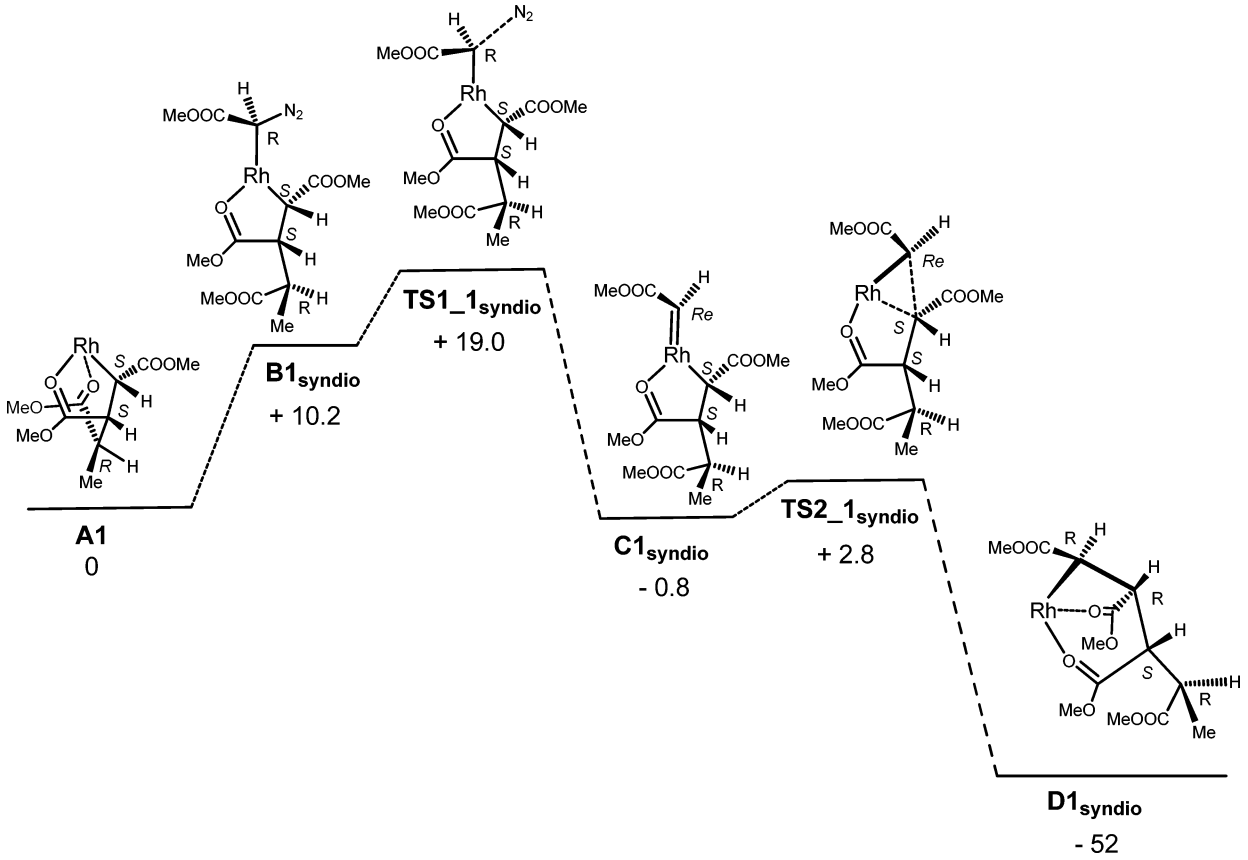

Figure 3. Calculated pathway for syndiotactic carbene insertion steps associated with (rate-determining) carbene formation steps from **A1** and MDA. The (cycloocta-2,6-dien-1-yl) ligand is omitted for clarity. Relative free energies (ΔG°_{298K}) in kcal mol^{-1} (b3-lyp, def2-TZVP, corrected for van der Waals interactions (disp3)).

MeOH-based termination/chain-transfer mechanism to those from species **A1**. In addition, we explored the effect of a chain error at the α-carbon of species **A1** on the propagation mechanism (section 2.6).

2.4. Propagation via Migratory Carbene Insertion Polymerization: Chain-End-Controlled Polymerization Leading to Syndiotactity. Once MDA adduct **B1** is formed, the carbene polymerization propagation steps essentially proceed via an expected migratory carbene insertion polymerization mechanism according to DFT. Propagation from **B1** proceeds by means of rate-limiting N_2 loss[57] via **TS1_1** (19.0 kcal mol^{-1}) to produce carbene intermediate **C1**, which undergoes migratory insertion into the Rh−C bond via a low-barrier transition state **TS2_1** to produce species **D1** having a one-carbon elongated polymeryl chain (see Figures 3 and 4). We explored both the syndiotactic insertion steps and formation of a stereoerror via an isotactic insertion step from **C1** in order to find a mechanistic explanation for the experimentally observed high syndiotacticity of the reaction. Syndiotactic insertion involves attack of the *re*-face of carbene intermediate **C** by the S-configured α-carbon atom of the growing chain (or, equivalently, *si*-face attack by an R-configured α-carbon atom), whereas a tacticity error can be induced by an isotactic insertion step involving *si*-face attack of on carbene intermediate **C1** by the S-configured α-carbon atom (see also Figure 5). The species $\mathbf{C1}_{\mathbf{syndio}}$ (Figures 3 and 6) is preorganized for syndiotactic insertion, although $\mathbf{C}_{\mathbf{iso}}$ (Figures 4 and 6) is preorganized for isotactic insertion. N_2-loss from $\mathbf{B1}_{\mathbf{syndio}}$ (via $\mathbf{TS1\_1}_{\mathbf{syndio}}$) and $\mathbf{B1}_{\mathbf{iso}}$ (via $\mathbf{TS1\_1}_{\mathbf{iso}}$) produces directly $\mathbf{C1}_{\mathbf{syndio}}$ and $\mathbf{C1}_{\mathbf{iso}}$, respectively. Species $\mathbf{B1}_{\mathbf{syndio}}$ is slightly (+1.1 kcal mol^{-1}) higher in energy than $\mathbf{B1}_{\mathbf{iso}}$, and also the **TS1_1** barrier on the syndiotactic pathway (referenced from species **A1**) is slightly higher (1.2 kcal mol^{-1}) than the one on the isotactic pathway. However, both these observations are hardly relevant because species $\mathbf{C1}_{\mathbf{iso}}$ and $\mathbf{C1}_{\mathbf{syndio}}$ are easily interconvertible through rotation about the Rh=C bond (low-barrier rotation barrier of +0.2 kcal mol^{-1} for syndio → iso and +4.9 kcal mol^{-1} for iso → syndio, see Figure 7). The stereospecificity of the carbene polymerization reaction is therefore mainly determined by the relative barriers of the subsequent low-barrier carbene insertion steps (Curtin−Hammet principle).

Due to the presence of a chiral (cycloocta-2,6-dien-1-yl) ligand on the catalyst, the tacticity of the polymer can in principle be controlled by the catalyst (site control) and does not necessarily have to be chain-end-controlled (see also Figure 5), as assumed in previous studies.[1−20] Site control may indeed play a role, as the DFT calculations show that the chiral cycloocta-2,6-dien-1-yl ligand affects the relative energy of $\mathbf{C1}_{\mathbf{iso}}$ versus $\mathbf{C1}_{\mathbf{syndio}}$ due to stabilizing interactions of the ester groups in the lower energy species $\mathbf{C1}_{\mathbf{iso}}$. Notably, this leads to a substantially *higher* $\mathbf{TS2\_1}_{\mathbf{iso}}$ barrier compared to $\mathbf{TS2\_1}_{\mathbf{syndio}}$. The energy difference between the $\mathbf{TS2\_1}_{\mathbf{syndio}}$ and $\mathbf{TS2\_1}_{\mathbf{iso}}$ barriers (6.5 kcal mol^{-1}) for the cationic [(cycloocta-2,6-dien-1-yl)Rh^{III}(alkyl)]$^+$ is actually much higher than previously calculated for carbene insertion at the neutral [(diene)-Rh^{I}(alkyl)] species (∼1 kcal mol^{-1}).[6] However, because carbene rotation is a low-barrier process, the ratio of

dx.doi.org/10.1021/cs500160c | ACS Catal. 2014, 4, 1376−1389

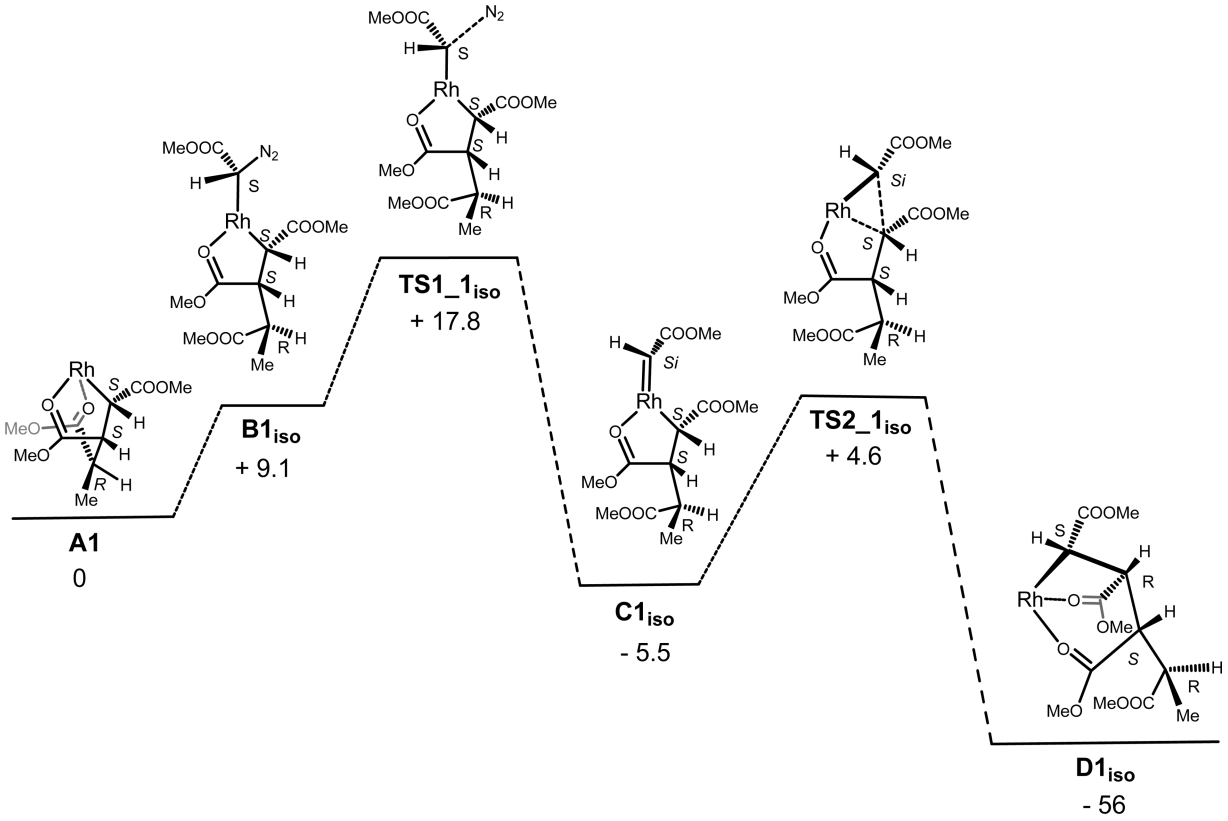

Figure 4. Calculated pathway for isotactic carbene insertion associated with (rate-determining) carbene formation steps from **A1** and MDA. The (cycloocta-2,6-dien-1-yl) ligand is omitted for clarity. Relative free energies (ΔG°_{298K}) in kcal mol^{-1} (b3-lyp, def2-TZVP, corrected for van der Waals interactions (disp3)).

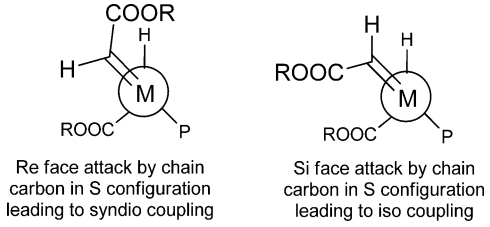

Figure 5. Newman projections of Rh-mediated carbene coordination before insertion into the polymer chain showing sterically preferred syndiotactic insertion (chain-end control). P = polymer chain. R = Me. Attack on the carbene *re*-face produces an R-configured α-carbon atom, whereas attack on the carbene *si*-face produces an S-configured α-carbon atom of the elongated growing chain.

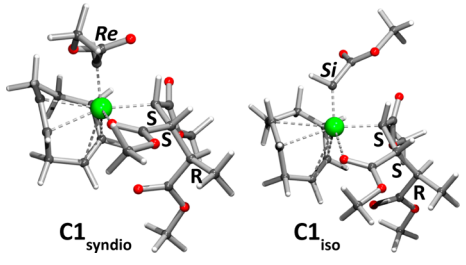

Figure 6. Structures of species **C**. Left: carbene unit preorganized for syndiotactic insertion (the ester unit is pointing to the front, the proton points backward). Right: carbene unit preorganized for syndiotactic insertion (proton pointing to the front, ester unit pointing backward).

syndiotactic versus isotactic chain propagation steps depends mostly on the relative barriers **TS2_1**$_{syndio}$ versus **TS2_1**$_{iso}$ relative to **C1**$_{iso}$ (see Figure 7). This leads to a preference for syndiotactic propagation based on steric repulsion between the ester moieties of the carbene monomer and the last inserted monomer of the chain. Hence, despite the chirality of the catalyst, the stereospecificity of the carbene polymerization reaction seems to be still largely chain-end-controlled. On this basis, the DFT calculations predict a moderate syndiospecificity ($k_{syndio}/k_{iso} \sim 21$). A steady state kinetic model including all calculated kinetic parameters (k_1, k_1', k_2, k_2', k_3, and k_3', see Figure 8) leads to $k_{syndio}/k_{iso} = 20.8$. A kinetic model neglecting the influence of k_1 and k_1' leads to similar results ($k_{syndio}/k_{iso} = 20.9$).[58] The experimental stereospecificity is higher (stereo-errors are hardly detectable in the obtained polymers), but the predicted trend is correct. Because the transition state energy differences are small, slight errors in the calculations easily lead to large deviations in predictions of the stereospecificity compared to experimental values. In that sense, predicting the stereospecificity of a polymerization reactions with DFT is associated with similar problems as predicting enantioselectivities (ee %) in catalysis.[59] The correctly predicted syndiospecific propagation is an important feature, answering the first mechanistic question posed in the introduction.

Species **D1**$_{syndio}$, formed after migratory insertion of the carbene moiety in **C1**$_{syndio}$ (via **TS2_1**$_{syndio}$), is in fact a one-carbon elongated enantiomer of **A2R′** and hence is an elongated (and enantiomeric) form of diastereomer **A2** rather than **A1** (see Figure 9).[61]

This is logical, because after each migratory insertion the configuration of the chiral α-carbon attached to Rh changes

dx.doi.org/10.1021/cs500160c | ACS Catal. 2014, 4, 1376−1389

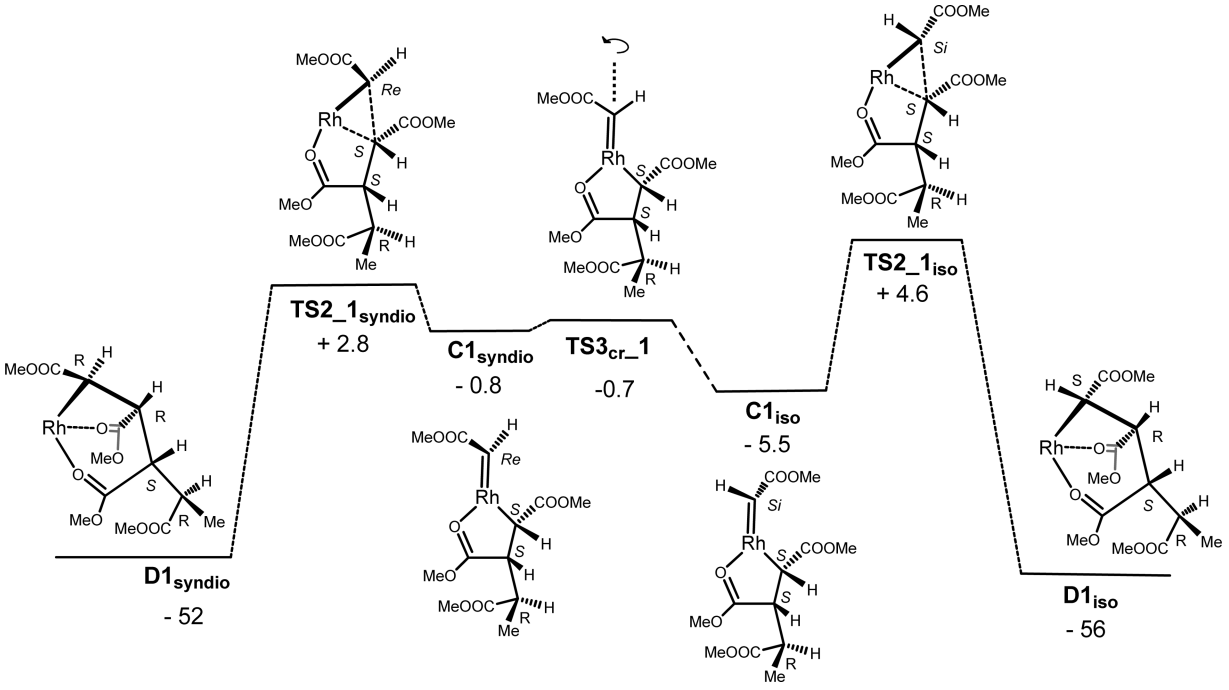

Figure 7. Chain-end control leading to syndiospecific propagation. Selectivity determining transition states **TS2_1**$_{syndio}$ and **TS2_1**$_{iso}$ preceded by carbenes **C1**$_{syndio}$ and **C1**$_{iso}$ in a rapid pre-equilibrium. The (cycloocta-2,6-dien-1-yl) ligand is omitted for clarity. Relative free energies (ΔG°_{298K}) in kcal mol^{-1} (b3-lyp, def2-TZVP, corrected for van der Waals interactions (disp3)).

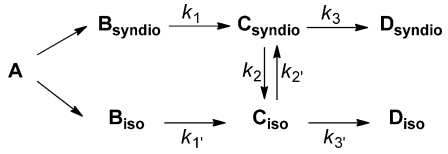

Figure 8. Selectivity of the syndiotactic over isotactic carbene insertion ($k_{syyndio}/k_{iso}$) depending on rate constants k_1, k_1', k_2, k_2', k_3, and k_3'.

from S to R or vice versa. The next propagation step might proceed directly from **D1**, but the species is likely to rearrange first to its more stable rotameric form **A2** (or actually its one-carbon elongated version, but this should not have any significant influence on the calculated energies and barriers).[60] To streamline the discussion and simplify the calculations, we therefore calculated the propagation steps for the next carbene insertion step to proceed from diastereomer **A2**.[60]

The subsequent propagation steps from diastereomer **A2** (to which MDA can only coordinate on the side of the $-CH_2-$ fragment of the cycloocta-2,6-dien-1-yl ligand) proceed in a very similar manner as from **A1**, with comparable energy barriers as well, albeit with absolute barriers that are somewhat higher than for the pathways from **A1**. The relative barrier of **TS2_2**$_{iso}$ compared to **TS2_2**$_{syndio}$ (Figure 10) is comparable to **TS2_1**$_{iso}$ versus **TS2_1**$_{syndio}$ (Figure 7), again predicting a preference for syndiotactic propagation. This is to be expected and is in fact a prerequisite for an insertion mechanism leading to syndiotactic carbene polymers.

The somewhat higher absolute transition state barriers observed for the propagation pathways from species **A2** are due to the increased steric hindrance of the $-CH_2-$ fragment in species **A2** being close to the substrate binding site as compared to the more open $-C_2H_4-$ moiety in **A1**.

Overall, the above DFT calculations show that propagation involving a migratory carbene insertion mechanism is certainly feasible for a cationic [(cycloocta-2,6-dien-1-yl)-Rh^{III}(polymeryl)]$^+$ species, and the computations are in agreement with the experimentally observed syndiotacticity of these polymerization reactions. However, the question why polymers with a high M_w are obtained is not yet clarified. To answer this question, we investigated the likely termination steps of the polymerization reaction, as discussed in the next sections.

2.5. Termination Processes. The last step in the polymerization process is termination, in which the active polymer chains are capped, preventing further chain growth. Typically, if termination is close (or even lower) in energy than propagation, short (low molecular weight) polymers or dimers are obtained. Detailed analysis of the experimental polymers obtained revealed that the polymers most likely terminate by protonation of the Rh−C bond of the active polymeryl chain by alcohols, thus leading to saturated polymer chain ends (polymeryl−CH(COOR)−CH$_2$(COOR)).[12] Chain termination by β-hydride elimination leading to unsaturated chain ends (polymeryl−C(COOR)═CH(COOR)) does not seem to play an important role in the mechanism. Previous DFT calculations on neutral [(diene)Rh^{I}(alkyl)] species demonstrated a low energy pathway for β-hydride elimination and could not explain the experimentally observed long polymers. Neutral [(diene)Rh^{I}(alkyl)] species are thus predicted to produce dimers or at best short, unsaturated oligomers as products (see Figure 11). This may explain the formation of the minor side products obtained in these reactions but not the main polymeric products. Rapid β-hydride elimination and reinsertion might occur for these species,[1,14,62] but this remained an unsatisfying explanation of the experimental results.

We therefore decided to perform new calculations on the termination steps using cationic [(cycloocta-2,6-dien-1-yl)-Rh^{III}(alkyl)]$^+$ species **A1** as a model for the active species

dx.doi.org/10.1021/cs500160c | ACS Catal. 2014, 4, 1376−1389

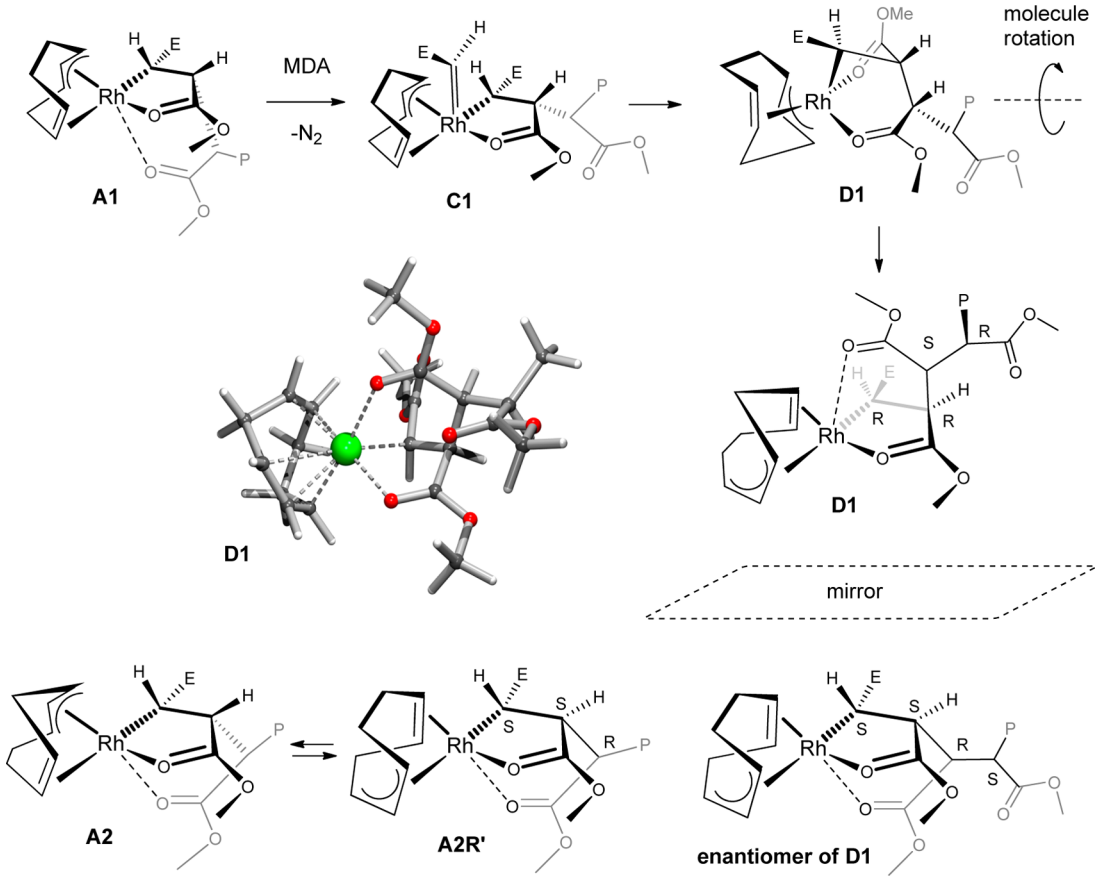

Figure 9. Species **D1**, with the alkyl of the polymer chain trans to the allyl moiety of the (cycloocta-2,6-dien-1-yl) ligand and its relation to species **A2R′** and **A2**.

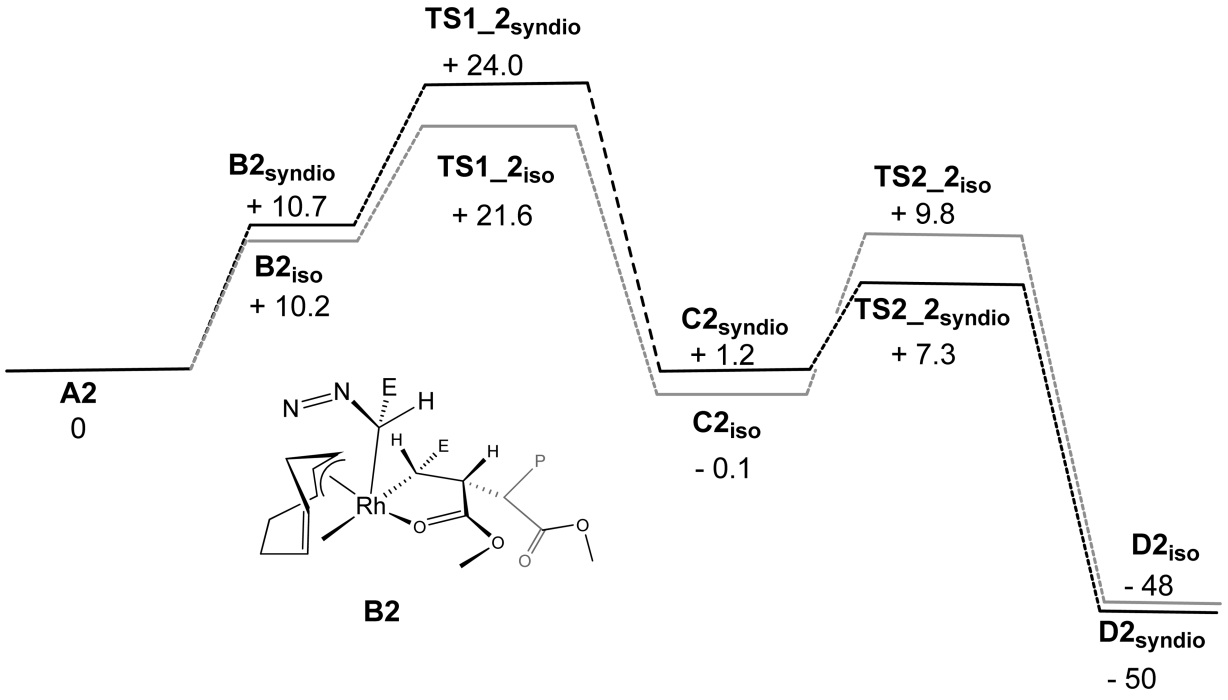

Figure 10. Calculated pathway for syndiotactic and isotactic carbene insertion associated with (rate-determining) carbene formation steps from **A2** and MDA. The (cycloocta-2,6-dien-1-yl) ligand is omitted for clarity. Relative free energies (ΔG°_{298K}) in kcal mol^{-1} (b3-lyp, def2-TZVP, corrected for van der Waals interactions (disp3)).

(based on the experimental results described in ref 20). We will first describe the calculated pathway for β-hydride elimination to compare the energy barrier with those of the propagation steps (section 2.5.1). In section 2.5.2, we will describe the

dx.doi.org/10.1021/cs500160c | ACS Catal. 2014, 4, 1376−1389

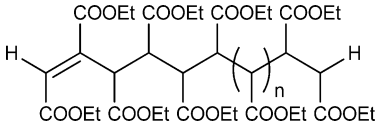

Figure 11. Unsaturated polymer resulting from β-hydride elimination.

calculated pathway for alcohol-mediated protonation of the active polymer chain, again to compare the barriers for termination and propagation.

2.5.1. Termination by β-hydride Elimination. The calculated pathway for β-hydride elimination at cationic [(cycloocta-2,6-dien-1-yl)Rh^{III}(alkyl)]$^+$ species **A1** and **A2** is shown in Figure 12.

The transition state barriers **TS4**$_{\beta\text{-H}}$**_1** (+22.2 kcal mol^{-1}) and **TS4**$_{\beta\text{-H}}$**_2** (+ 25.1 kcal mol^{-1}) are much higher than the highest barriers on the propagation pathways from **A1** and **A2**, respectively (see Figures 3 and 4). These energy barriers are likely too high to represent a reasonable termination pathway from cationic [(cycloocta-2,6-dien-1-yl)Rh^{III}(polymeryl)]$^+$ species. Furthermore, formation of the hydride species **E**$_{\text{B–H}}$**_1** and **E**$_{\text{B–H}}$**_2** is highly endergonic in both cases (+21.7 kcal mol^{-1} from **A1**, +24.8 kcal mol^{-1} from **A2**, respectively), and these species have their unsaturated "terminated" polymer chain still coordinated to rhodium in a chelating fashion with both an ester carbonyl and the olefinic double bond in cis position to the hydride. This makes olefin reinsertion into the Rh–H bond (to regenerate **A1** or **A2**) a facile process, which is more likely to occur than dissociation of an unsaturated polymeryl–C(COOR)=CH(COOR) chain. This high energy pathway for chain transfer or chain termination via β-hydride elimination helps to explain why unsaturated polymer chains are not obtained experimentally.

2.5.2. Alcohol-Mediated Chain Transfer. Another way to terminate polymer growth is through protonation of the polymer chain by an alcohol. In refs 12 and 20, experimental proof is provided for this mechanism. DFT calculations support these experimental data (see Figure 13). To minimize computation time, we evaluated this pathway only from species **A1**.

In agreement with the experimental observations showing that the nucleophilicity of the alcohol plays a role,[12] the calculated alcohol-mediated chain-transfer process proceeds via initial coordination of the alcohol moiety to the Rh center. The catalyst has a similar affinity for MeOH as for MDA, although coordination of methanol to the Rh^{III} center of the cationic [(cycloocta-2,6-dien-1-yl)Rh^{III}(alkyl)]$^+$ species **A1** is slightly less endergonic (7.6 kcal mol^{-1}).

MeOH-mediated chain transfer must involve protonation of the growing alkyl chain at some point. However, direct proton transfer from the coordinated MeOH moiety in **F** to the Rh–C bond is troublesome. We were unable to find a transition state for proton transfer from the coordinated MeOH molecule directly to the Rh–C bond of the growing chain without invoking an additional MeOH molecule. The process is facilitated when proceeding via a H-bonding proton transfer network involving an additional MeOH molecule,[64] but even then the transition state for net proton transfer from the coordinated alcohol moiety to the Rh–C bond of **F** is still very high ($\Delta G^{\ddagger}$ = 54 kcal mol^{-1}; $\Delta H^{\ddagger}$ = 34 kcal mol^{-1}) and clearly out of range for reactions at room temperature. Therefore, the molecule has to rearrange to species **G** having an O-

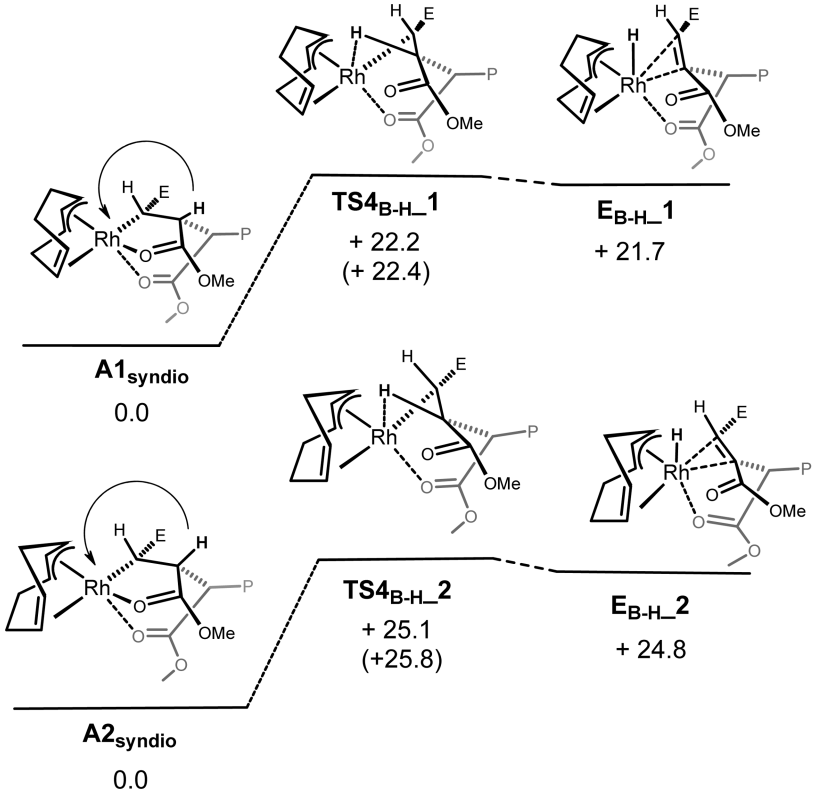

Figure 12. Calculated pathway for β-hydride elimination at cationic [(cycloocta-2,6-dien-1-yl)Rh^{III}(alkyl)]$^+$ species **A1** (top) and **A2** (bottom). The (cycloocta-2,6-dien-1-yl) ligand is omitted for clarity. Relative free energies (ΔG°_{298K}) in kcal mol^{-1}, relative enthalpies (ΔH°_{298K}) between brackets (b3-lyp, def2-TZVP, corrected for van der Waals interactions (disp3)).

dx.doi.org/10.1021/cs500160c | *ACS Catal.* 2014, 4, 1376–1389

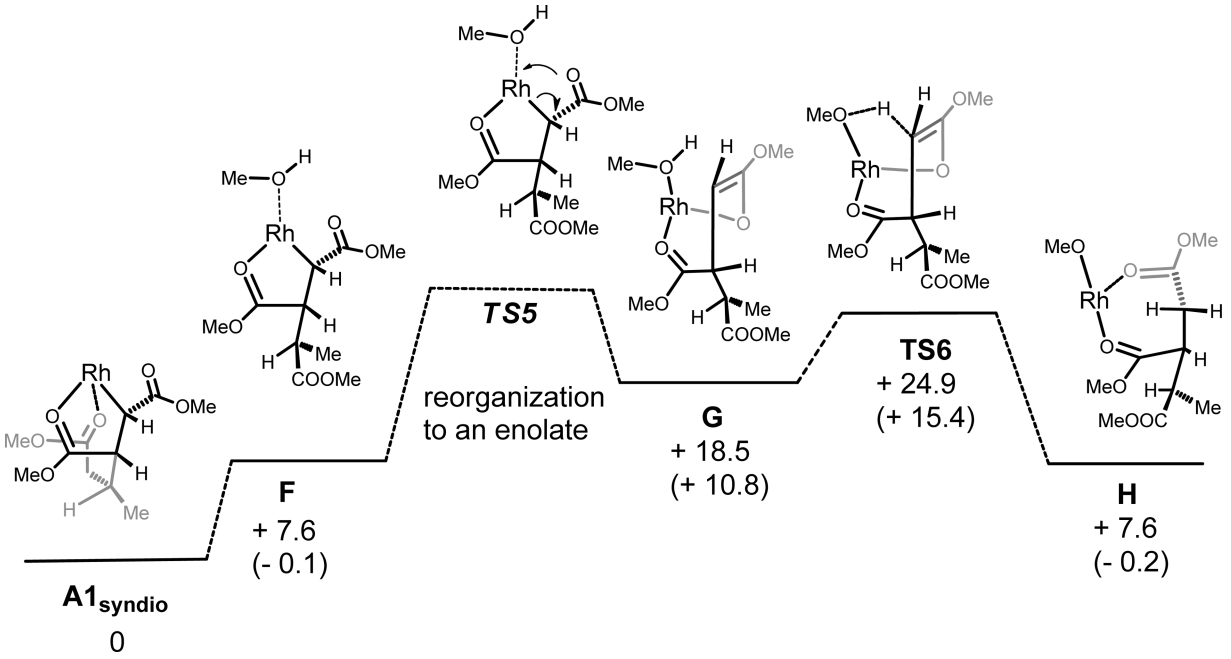

Figure 13. Calculated pathway for intermolecular proton transfer from a coordinated alcohol moiety to the polymer chain, leading to chain termination via protonation of the Rh−C bond. The (cycloocta-2,6-dien-1-yl) ligand is omitted for clarity. Relative free energy (ΔG°_{298K}) in kcal mol^{-1}, relative enthalpy (ΔH°_{298K}) between brackets (b3-lyp, def2-TZVP, corrected for van der Waals interactions (disp3)).

coordinated enolate moiety to allow efficient proton transfer from MeOH to terminate the polymer chain.[63] Formation of isomer **G** from **F** is endergonic by 11 kcal mol^{-1}. Proton transfer from MeOH to the enolate carbon in G proceeds via transition state **TS6**, (+6 kcal mol^{-1} higher than **G**), representing an overall free energy barrier of +24.9 kcal mol^{-1}. This barrier is somewhat higher than the barrier for β-hydride elimination from **A1** (22.2 kcal mol^{-1}). However, the entropy contributions to the DFT-calculated free-energy barrier **TS6** in the gas phase are overestimated (in fact, the entropy correction terms used here to translate the DFT gas phase data into free energies more relevant for solution chemistry may already be small; see the Computational Details section). In the actual solution mixtures, the reactions are performed with a large excess of alcohol. Hence, the translational entropy contributions to the free-energy barrier of the experimental alcohol-mediated chain-transfer pathway are much smaller ($\Delta G = \Delta G^{\ddagger} + RT\ln Q$), so when a large excess of MeOH is used, the corrected free-energy barrier lowers, and this value should be compared with the free-energy barrier for β-hydride elimination. The actual free-energy barrier for MeOH mediated chain-transfer in solution under nonstandard conditions should therefore be somewhere in between +25 ($\Delta G^{\ddagger}$) and +15 kcal mol^{-1} ($\Delta H^{\ddagger}$), hence most likely lower than β-hydride elimination ($\Delta H^{\ddagger}$ = 22.4 kcal mol^{-1}).[65] Furthermore, β-hydride elimination is, overall, a strongly endothermic process (ΔG° = 21.7 kcal mol^{-1} from **A1**) with a low-barrier transition state for the reverse reaction (see Figure 12), whereas alcohol-mediated chain transfer is exothermic (ΔH° = −0.2 kcal mol^{-1}). Taken together, the computed alcohol-mediated chain-transfer pathway is both kinetically and thermodynamically preferred over β-hydride elimination, in good agreement with the experimental observations.[12]

The free-energy barrier for alcohol-mediated chain transfer is higher than the barrier for chain propagation. These barriers can be directly compared because both the alcohol and the diazo substrate are used in a large excess compared to the (active) catalyst (similar deviations in the translational entropy contributions). Hence, in agreement with the experimental observations,[12] chain propagation is much faster than alcohol-mediated chain-transfer. Experimentally, alcohol-mediated chain-transfer starts to compete significantly with chain propagation only when using relatively high alcohol concentrations. This is in agreement with a large entropy contribution to the computed standard free-energy barrier ($\Delta G^{\ddagger}$) for alcohol-mediated chain transfer in combination with a lower translational entropy contribution when increasing the alcohol concentration.

The pathway shown in Figure 13 leaves a Rh−OMe fragment in species **H**, from which a new polymer-chain can start growing in a later stage. The terminated polymer chain having a saturated chain end (CH_3−polymeryl−CH(COOR)−CH_2(COOR)) is initially still coordinated to Rh but only with one of its carbonyl moieties. This fragment should thus be easily displaceable from **H** once a new chain starts growing. The calculated pathway therefore readily explains the experimentally observed chain-transfer role of alcohols.

2.6. Effect of Stereoerrors on the Propagation Mechanism and the Stereoerror Repair Mechanism. We further investigated chain propagation from an analogue of **A1** containing a stereoerror at the α-carbon atom of the [{CH(COOMe)}$_3$Me] moiety with DFT. This [(cycloocta-2,6-dien-1-yl)Rh^{III}({CH(COOMe)}$_3$Me]$^+$ species **A3** has an RSR configured chain instead of the SSR configuration in **A1**. MDA binding at syndiotactic **A1** leads to formation of adduct **B1**, which upon N_2 loss produces the discrete carbene intermediate **C1** (Figure 14, left). Exploring the same reaction at the nonsyndiotactic analogue **A3** containing an RSR configuration of the −{CH(COOMe)}$_3$Y moiety gives markedly different results (Figure 15). First of all, MDA has to bind to a sterically more encumbered position from which the substrate is sterically isolated from the ester moiety attached to the α-

dx.doi.org/10.1021/cs500160c | ACS Catal. 2014, 4, 1376−1389

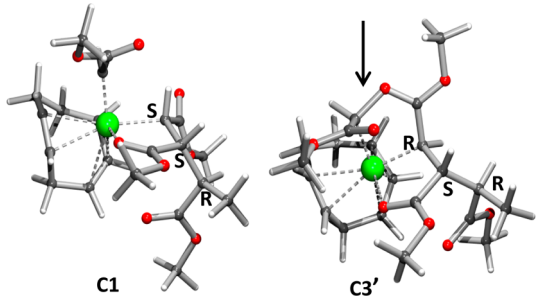

Figure 14. Effect of tacticity errors on the polymerization reaction. Left: the discrete carbene intermediate **C1** is stable because the oxygen-ylide-formation is not possible in the syndiotactic SSR configuration of the $-\{CH(COOMe)\}_3Me$ moiety. Right: in the nonsyndiotactic analogue carbene formation leads to spontaneous attack of the ester carbonyl attached to the α-carbon of the RSR-configured $-\{CH(COOMe)\}_3Y$ moiety producing low-energy species **C3′**.

carbon of the RSR-configured $-\{CH(COOMe)\}_3Y$ moiety (**B3**). More importantly, the carbene species **C3** generated from this intermediate tends to be unstable and easily converges (in a virtual barrier-less process) to an oxygen-ylide-structure **C3′**, in which the ester moiety attached to the α-carbon of the RSR-configured $-\{CH(COOMe)\}_3Y$ chain has attacked the carbene unit (Figure 14, right).

This bond formation (C−O bond distance of 1.497 Å, see Figure 14) substantially stabilizes the species (**C3′** is 22.0 kcal mol^{-1} lower in energy than **C1**). This means that stereoerrors induced at the α-carbon atom should substantially reduce the rate of the subsequent propagation reaction via carbene insertion compared to chain propagation from $[(cycloocta\text{-}2,6\text{-}dien\text{-}1\text{-}yl)Rh^{III}(\{CH(COOMe)\}_3P)]^+$ species without such stereoerrors. Although expected to reduce the reaction rate substantially, ylide formation is reversible, and the overall strongly exothermic carbene polymerization process does allow for a repair mechanism involving syndiotactic carbene insertion in the Rh−C bond (see Figure 15). The k_{syndio}/k_{iso} ratio (~21) reported in section 2.4 is high enough to correct for such "errors" to result in mainly syndiotactic chain growth.

2.7. Possible Explanations for the Experimentally Observed Low Initiation Efficiencies. Chain errors generated during carbene polymerization should have a similar effect on all active syndiotactic growing polymer chains (although it may potentially affect the molecular weight distribution over time, as observed in the experimental polymerization reactions). Chain errors such as those explored for species **A3** likely also have a strong influence on the initiation efficiency of the reaction, because they should clearly slow chain propagation from nonsyndiotactic chains. In the experimental polymerization reactions, we consistently observed that only a minor amount of the Rh species becomes active as a polymerization catalyst (initiation efficiencies typically <10%, neglecting chain-transfer effects). Experimental data could thus far not provide a satisfying explanation for this behavior. Although highly syndiotactic polymers are obtained in the experimental reactions, ill-defined atactic oligomers are also formed in the beginning of the reaction. Hence, the initial cationic $[(cycloocta\text{-}2,6\text{-}dien\text{-}1\text{-}yl)Rh^{III}(\{CH(COOMe)\}_3Y)]^+$ species (Y = H, OH, OR) formed during the catalyst activation process, which are required to initiate chain growth, do not necessarily all contain a syndiotactic $-\{CH(COOMe)\}_3$ growing-chain fragment. In fact, it is very unlikely that the first three carbene insertion reactions during the catalyst activation process generate only syndiotactic $-\{CH(COOMe)\}_3Y$ moieties, because at this stage of the reaction, the initiating chain is yet too short to benefit from the same

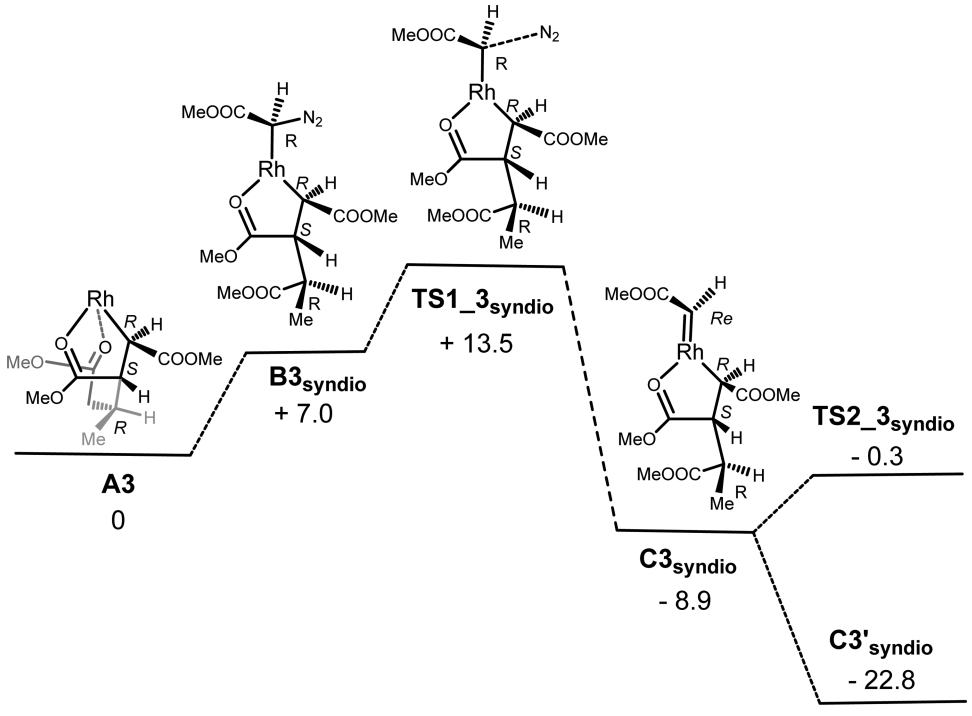

Figure 15. Calculated pathway for syndiotactic carbene insertion associated with (rate determining) carbene formation steps from **A3** and MDA. The (cycloocta-2,6-dien-1-yl) ligand is omitted for clarity. Relative free energies ($\Delta G°_{298K}$) in kcal mol^{-1} (b3-lyp, def2-TZVP, corrected for van der Waals interactions (disp3)).

dx.doi.org/10.1021/cs500160c | ACS Catal. 2014, 4, 1376−1389

protecting chelating properties of the carbonyl moieties as in **A1** or **A2**. The carbonyl moieties of the initiating growing chain fragment either do not or only partially coordinate to Rh^{III}, and any chelating properties of the chain at this stage are different and weaker than those in species **A1** or **A2**. Such short, initiating growing-chain fragments have much more flexibility to rotate around the Rh−C bond and are much less sterically hindered at the metal site (at this stage) compared to **A1** or **A2**, thus leaving room for MDA to bind at multiple positions. The formation of a syndiotactic $-\{CH(COOMe)\}_3Y$ moiety in the first three insertion steps must therefore be (at least in part) based on chance, leading to a more or less statistical distribution of $-\{CH(COOMe)\}_3Y$ chain configurations (RRR, RRS, RSR, RSS, SSR, SRS, of which only SSR and RRS are syndiotactic). In itself, the k_{syndio}/k_{iso} ratio (~21) calculated in section 2.4 should be high enough to correct for these initial "errors" to produce syndiotactic chain growth later in the reaction. However, chain growth from already syndiotactic chains should start easily and should proceed much faster than from nonsyndiotactic chains, so that much of the MDA substrate will be already consumed before chain growth from the initial nonsyndiotactic species becomes relevant. If we assume that the initial catalyst activation steps are purely statistical (RRR, RRS, RSR, RSS, SSR, SRS), only 33% of syndiotactic SSR and RRS species are generated initially. This may well contribute to the experimentally observed low initiation efficiencies of these catalyst in carbene polymerization reactions. In addition, ineffective formation of the cationic $[(cycloocta\text{-}2,6\text{-}dien\text{-}1\text{-}yl)Rh^{III}(\{CH(COOMe)\}_3Y)]^+$ species from the catalyst precursors used will further reduce the overall initiation efficiency.

3. CONCLUSIONS

The DFT-computed pathways for chain propagation and chain transfer reveal important details about carbene polymerization using cationic $[(cycloocta\text{-}2,6\text{-}dien\text{-}1\text{-}yl)Rh^{III}(alkyl)]^+$ species, and with this new insight, we were able to answer the four questions mentioned in the introduction.

Chain propagation at these species is clearly competitive with β-hydride elimination, explaining the formation of high molecular weight polymers. These results are in agreement with experimental observations and clearly in contrast with previously reported DFT calculations using neutral $[(diene)Rh^{I}(alkyl)]$ species, which failed to explain the formation of long polymers. In analogy with previous calculations using neutral $[(diene)Rh^{I}(alkyl)]$ species, chain propagation at cationic $[(cycloocta\text{-}2,6\text{-}dien\text{-}1\text{-}yl)Rh^{III}(alkyl)]^+$ species is still chain-end-controlled, leading to a clear preference for syndiotactic polymerization.

Chain transfer involving alcohol-mediated protonolysis is computed to be a more favorable pathway than β-hydride elimination. This explains the formation of saturated, alcohol-terminated RO−polymeryl−$CH(COOR)-CH_2(COOR)$ chains rather than unsaturated (H−polymeryl-$CH(COOR)=CH(COOR)$ chains. Furthermore, in good agreement with previously reported experimental observations showing that the nucleophilicity of the alcohol plays a role,[12] the calculated alcohol-mediated chain-transfer process proceeds via initial coordination of the alcohol moiety to the Rh center. Protonolysis of the growing chain requires rearrangement of the Rh−polymeryl chain to an O-bound Rh−enolate, followed by rapid proton-transfer from the coordinated alcohol moiety to the enolate carbon moiety. This process has a higher barrier than chain propagation but a lower barrier than β-hydride elimination.

Chain propagation from species with a stereoerror at the α-carbon atom of the growing chain is substantially slowed compared to propagation from syndiotactic species without stereoerrors. This effect arises from attack of the carbonyl group of the α-ester moiety on the carbene unit, stabilizing the propagating species in an unfavorable off-cycle equilibrium. This process is reversible, allowing a stereorepair mechanism. Similar effects may play a role in explaining the low initiation efficiency of the catalyst. Statistically, only 33% of the initially formed triad chains are formed in a syndiotactic manner during the activation process of the catalyst. Much faster propagation from these syndiotactic chains compared to nonsyndiotactic chains may well contribute to the experimentally observed low initiation efficiencies of these catalysts in carbene polymerization reactions.

With these new computational insights, in combination with the experimental results described in earlier reports,[12,20] the mechanism of the polymerization reaction is largely clarified.

4. COMPUTATIONAL DETAILS

All DFT geometry optimizations were carried out with the Turbomole program[66−69] coupled to the PQS Baker optimizer[70,71] via the BOpt package.[72] Geometries were fully optimized as minima or transition states at the b3-lyp level[73,74] using the Turbomole (polarized triple-ζ) def2-TZVP basis[75−80] (small-core pseudopotential at Rh[77]). Grimme's dispersion corrections (D3 version, implemented with the keyword disp3 in Turbomole) were applied in all geometry optimizations.[81] All minima (no imaginary frequencies) and transition states (one imaginary frequency) were characterized by calculating the Hessian matrix. ZPE and gas-phase thermal corrections (entropy and enthalpy, 298 K, 1 bar) from these analyses were calculated. The relative (free) energies obtained from these calculations are reported in the main text of this paper. The nature of the transition states was confirmed by IRC calculations. Optimized geometries are visualized with the PLATON[82] program (rendered with POVRAY).

By calculation of the partition function of the molecules in the gas phase, the entropy of dissociation or coordination for reactions in solution is overestimated (overestimated translational entropy terms in the gas phase compared to solutions). For reactions in "solution", we therefore corrected the Gibbs free energies for all steps involving a change in the number of species (except the N_2 loss step following **TS1**). Several methods have been proposed for corrections of gas phase to solution phase data. The minimal correction term is a correction for the condensed phase (CP) reference volume (1 L mol^{-1}) compared to the gas phase (GP) reference volume (24.5 L mol^{-1}). This leads to an entropy correction term ($S_{CP} = S_{GP} + Rln\{1/24.5\}$ for all species, affecting relative free energies (298 K) of all associative (−2.5 kcal mol^{-1}) and dissociative steps (+2.5 kcal mol^{-1}),[83] which is the correction term used in this paper. According to some authors, this correction term is too small, and larger correction terms (even up to 6.0 kcal mol^{-1}) have been suggested in other studies.[84,85] Which correction term is best remains debatable, and for this reason we supplied a separate energy spreadsheet to the Supporting Information. If so desired, this allows the reader to correct the free energies with different correction terms by simply changing a single entry.

■ ASSOCIATED CONTENT

Supporting Information

Cartesian coordinates of the stationary points and transition states, kinetic equations used to calculate the syndio/iso ratio, spreadsheet containing the computed SCF energies, ZPE corrections, enthalpies, entropies, and (entropy-corrected) free

dx.doi.org/10.1021/cs500160c | ACS Catal. 2014, 4, 1376−1389

energies. This information is available free of charge via the Internet at http://pubs.acs.org/.

AUTHOR INFORMATION

Corresponding Author

*Email: b.debruin@uva.nl. Fax: (+31) 20 525 5604. Tel.: (+)31 20 525 6495.

Notes

The authors declare no competing financial interest.

ACKNOWLEDGMENTS

This research was supported by the European Research Council (ERC Grant Agreement 202886-CatCIR), The Netherlands Organisation for Scientific Research (NWO), and the University of Amsterdam.

REFERENCES

(1) Jellema, E.; Jongerius, A. L.; Reek, J. N. H.; de Bruin, B. *Chem. Soc. Rev.* **2010**, *39*, 1706−1723.

(2) Franssen, N. M. G.; Walters, A. J. C. *Catal. Sci. Technol.* **2011**, *1*, 153−165.

(3) Ihara, E. *Adv. Polym. Sci.* **2010**, *231*, 191−231.

(4) Hetterscheid, D. G. H.; Hendriksen, C.; Dzik, W. I.; Smits, J. M. M.; van Eck, E. R. H.; Rowan, A. E.; Busico, V.; Vacatello, M.; Van Axel Castelli, V.; Segre, A.; Jellema, E.; Bloemberg, T. G.; de Bruin, B. *J. Am. Chem. Soc.* **2006**, *128*, 9746−9752.

(5) Noels, A. F. *Angew. Chem., Int. Ed.* **2007**, *46*, 1208−1210.

(6) Jellema, E.; Budzelaar, P. H. M.; Reek, J. N. H.; de Bruin, B. *J. Am. Chem. Soc.* **2007**, *129*, 11631−11640.

(7) Rubio, M.; Jellema, E.; Siegler, M. A.; Spek, A. L.; Reek, J. N. H.; de Bruin, B. *Dalton Trans.* **2009**, *41*, 8970−8976.

(8) Jellema, E.; Jongerius, A. L.; van Ekenstein, G. A.; Mookhoek, S. D.; Dingemans, T. J.; Reingruber, E. M.; Chojnacka, A.; Schoenmakers, P. J.; Sprenkels, R.; van Eck, E. R. H.; Reek, J. N. H.; de Bruin, B. *Macromolecules* **2010**, *43*, 8892−8903.

(9) Franssen, N. M. G.; Reek, J. N. H.; de Bruin, B. *Polym. Chem.* **2011**, *2*, 422−431.

(10) Finger, M.; Reek, J. N. H.; de Bruin, B. *Organometallics* **2011**, *30*, 1094−1101.

(11) Finger, M.; Lutz, M.; Reek, J. N. H.; de Bruin, B. *Eur. J. Inorg. Chem.* **2012**, *9*, 1437−1444.

(12) Walters, A. J. C.; Jellema, E.; Finger, M.; Aarnoutse, P.; Smits, J. M. M.; Reek, J. N. H.; de Bruin, B. *ACS Catal.* **2012**, *2*, 246−260.

(13) Dzik, W. I.; Zhang, X. P.; de Bruin, B. *Inorg. Chem.* **2011**, *50*, 9896−9903.

(14) Franssen, N. M. G.; Finger, M.; Reek, J. N. H; de Bruin, B. *Dalton Trans.* **2013**, *42*, 4139−4152.

(15) Franssen, N. M. G.; Reek, J. N. H; de Bruin, B. *Dalton Trans.* **2013**, *42*, 9058−9068.

(16) Franssen, N. M. G.; Remerie, K.; Macko, T.; Reek, J. N. H.; de Bruin, B. *Macromolecules* **2012**, *45*, 3711−3721.

(17) Franssen, N. M. G.; Reek, J. N. H; de Bruin, B. *Chem. Soc. Rev.* **2013**, *42*, 5809−5832.

(18) Reingruber, E. M.; Chojnacka, A.; Jellema, E.; de Bruin, B.; Buchberger, W.; Schoenmakers, P. J. *J. Chromatogr. A* **2012**, *1255*, 259−266.

(19) Franssen, N. M. G.; Ensing, B.; Hegde, M.; Dingemans, T.; Norder, B.; Picken, S. J.; Alberda van Ekenstein, G. O. R.; van Eck, E.; Elemans, J. A. A. W.; Vis, M.; Reek, J. N. H.; de Bruin, B. *Chem.—Eur. J.* **2013**, *19*, 11577−11589.

(20) Walters, A. J. C.; Troeppner, O.; Ivanović-Burmazović, I.; Tejel, C.; del Río, M. P.; Reek, J. N. H.; de Bruin, B. *Angew. Chem., Int. Ed.* **2012**, *51*, 5157−5161.

(21) Ihara, E.; Ishiguro, Y.; Yoshida, N.; Hiraren, T.; Itoh, T.; Inoue, K. *Macromolecules* **2009**, *42*, 8608−8610.

(22) Bantu, B.; Wurst, K.; Buchmeiser, M. R. *J. Organomet. Chem.* **2007**, *692*, 5272−5278.

(23) Ihara, E.; Hiraren, T.; Itoh, T.; Inoue, K. *Polym. J.* **2008**, *40*, 1094−1098.

(24) Ihara, E.; Hiraren, T.; Itoh, T.; Inoue, K. *J. Polym. Sci., Part A: Polym. Chem.* **2008**, *46*, 1638−1648.

(25) Ihara, E.; Goto, Y.; Itoh, T.; Inoue, K. *Polym. J.* **2009**, *41*, 1117−1149.

(26) Ihara, E.; Haida, N.; Iio, M.; Inoue, K. *Macromolecules* **2003**, *36*, 36−41.

(27) Ihara, E.; Nakada, A.; Itoh, T.; Inoue, K. *Macromolecules* **2006**, *39*, 6440−6444.

(28) Ihara, E.; Fujioka, M.; Haida, N.; Itoh, T.; Inoue, K. *Macromolecules* **2005**, *38*, 2101−2108.

(29) Shea, K. J.; Busch, B. B.; Paz, M. M. *Angew. Chem., Int. Ed.* **1998**, *37*, 1391−1393.

(30) Busch, B. B.; Paz, M. M.; Shea, K. J.; Staiger, C. L.; Stoddard, J. M.; Walker, J. R.; Zhou, X.-Z.; Zhu, H. *J. Am. Chem. Soc.* **2002**, *124*, 3636−3646.

(31) Sulc, R.; Zhou, X.; Shea, K. J. *Macromolecules* **2006**, *39*, 4948−4952.

(32) Bai, J.; Shea, K. J. *Macromolecules* **2006**, *39*, 7196−7198.

(33) Bai, J.; Burke, L. D.; Shea, K. J. *J. Am. Chem. Soc.* **2007**, *129*, 4981−4991.

(34) Wang, J.; Horton, J. H.; Liu, G.; Lee, S.-Y.; Shea, K. J. *Polymer* **2007**, *48*, 4123−4129.

(35) Luo, J.; Shea, K. J. *Acc. Chem. Res.* **2010**, *43*, 1420−1433.

(36) Luo, J.; Lu, F. F.; Shea, K. J. *ACS Macro Lett.* **2012**, *1*, 560−563.

(37) Olivos Suarez, A. I.; del Río, M. P.; Remerie, K.; Reek, J. N. H.; de Bruin, B. *ACS Catal.* **2012**, *2*, 2046−2059.

(38) Syndiotactic polymers arise if the last inserted monomers have alternating R and S configurations (IUPAC definition). This leads to a polymer chain with all substituents pointing to the same side along the polymer chain when projected in a regular zigzag conformation when formed via a syndiotactic C1 polymerization process. This contrasts with syndiotactic olefin polymerization, which leads to a polymer having its substituents in an alternating front−back orientation along the zigzag projected chain. The difference is a direct result of inserting C1 monomers instead of C2 monomers.

(39) de Bruin, B.; Boerakker, M. J.; Donners, J. J. J. M.; Christiaans, B. E. C.; Schlebos, P. P. J.; de Gelder, R.; Smits, J. M. M.; Spek, A. L.; Gal, A. W. *Angew. Chem., Int. Ed.* **1997**, *36*, 2063−2067.

(40) de Bruin, B.; Brands, J. A.; Donners, J. J. J. M.; Donners, M. P. J.; de Gelder, R.; Smits, J. M. M.; Gal, A. W.; Spek, A. L. *Chem.—Eur. J.* **1999**, *5*, 2921−2936.

(41) de Bruin, B.; Budzelaar, P. H. M.; Gal, A. W. *Angew. Chem., Int. Ed.* **2004**, *43*, 4142−4157.

(42) de Bruin, B.; Peters, T. P. J.; Thewissen, S.; Blok, A. N. J.; Wilting, J. B. M.; de Gelder, R.; Smits, J. M. M.; Gal, A. W. *Angew. Chem., Int. Ed.* **2002**, *41*, 2135−2138.

(43) de Bruin, B.; Boerakker, M. J.; Verhagen, J. A. W.; de Gelder, R.; Smits, J. M. M.; Gal, A. W. *Chem.—Eur. J.* **2000**, *6*, 298−312.

(44) de Bruin, B.; Peters, T. P. J.; Wilting, J. B. M.; Thewissen, S.; Smits, J. M. M.; Gal, A. W. *Eur. J. Inorg. Chem.* **2002**, *10*, 2671−2680.

(45) de Bruin, B.; Boerakker, M. J.; de Gelder, R.; Smits, J. M. M.; Gal, A. W. *Angew. Chem., Int. Ed.* **1999**, *38*, 219−222.

(46) Hetterscheid, D. G. H.; de Bruin, B. *J. Mol. Catal. A: Chem.* **2006**, *251*, 291−296.

(47) Hetterscheid, D. G. H.; Kaiser, J.; Reijerse, E.; Peters, T. P. J.; Thewissen, S.; Blok, A. N. J.; Smits, J. M. M.; de Gelder, R.; de Bruin, B. *J. Am. Chem. Soc.* **2005**, *127*, 1895−1905.

(48) Hetterscheid, D. G. H.; Bens, M.; de Bruin, B. *Dalton Trans.* **2005**, *5*, 979−984.

(49) Hetterscheid, D. G. H.; de Bruin, B.; Smits, J. M. M.; Gal, A. W. *Organometallics* **2003**, *22*, 3022−3024.

(50) Jellema, E.; Jongerius, A. L.; Walters, A. J. C.; Smits, J. M. M.; Reek, J. N. H.; de Bruin, B. *Organometallics* **2010**, *29*, 2823−2826..

(51) de Bruin, B.; Hetterscheid, D. G. H. *Eur. J. Inorg. Chem.* **2007**, *2*, 211−230.

(52) van Leeuwen, P. W. N. M. *Homogeneous Catalysis, Understanding the Art*; Kluwer Acedemic Publishers: Dordrecht, The Netherlands, 2004.
(53) Anslyn, E. V.; Dougherty, D. A. *Modern Physical Organic Chemistry*; University Science Books: Sausalito, California, 2004.
(54) Atkins, P.; Overton, T.; Rourke, J.; Weller, M.; Armstrong, F.; Hagerman, M.*Shriver & Atkins' Inorganic Chemistry*, 5th ed.; Oxford University Press: Oxford, U.K., 2010.
(55) Fast ligand dissociation from rhodium(III) typically requires weak σ-donors and/or trans ligands with strong trans influence. de Bruin, B.; Verhagen, J. A. W.; Schouten, C. H. J.; Gal, A. W.; Feichtinger, D.; Plattner, D. A. *Chem.—Eur. J.* **2001**, *7*, 416−422.
(56) Transition states involving simultaneous rotation of all ligand atoms of a ligand with a low symmetry are difficult to locate due to poorly developed constrained geometry algorithms for such movements.
(57) Cohen, R.; Rybtchinski, B.; Gandelman, M.; Rozenberg, H.; Martin, J. M. L.; Milstein, D. *J. Am. Chem. Soc.* **2003**, *125*, 6532−6546.
(58) Strictly speaking, multiple isotactic insertion steps producing an isotactic chain analogue of **A1** (i.e., with an SRR-configured triad coordinated to rhodium instead of an SSR-configured triad) could lead to somewhat different isotactic insertion barriers than calculated here for an isotactic insertion step leading a stereoerror in an otherwise syndiotactic growing chain. This was not evaluated computationally, but steric effects introduced by changing the configuration of C2 of the growing chain from S to R are expected to be small. The effect of a chain error at the C1-position on subsequent propagation steps is evaluated in section 2.6.
(59) García, J. I.; Jiménez-Osés, G.; Mayoral, J. A. *Chem.—Eur. J.* **2011**, *17*, 529−539.
(60) Although **A2** formed from **D1** should in fact have one extra carbene unit inserted into the polymer chain, this extra moiety is positioned more than 4.90 Å away from the active site and hence will not affect the propagation barriers at all. Hence, the simplified $[(\text{cycloocta-2,6-dien-1-yl})\text{Rh}^{\text{III}}(\{\text{CH}(\text{COOMe})\}_3\text{CH}_3)]^+$ version of species **A2** functions as a simplified model to study the next carbene insertion step.
(61) To be precise, ligand rotation in **D1** to produce its most stable rotameric form produces an enantiomer of rotamer **A2R′**, which (after ligand rotation) thus produces an enatiomer of **A2** drawn in Figure 1 (see also Figure 9). Obviously, enantiomers of **A2** (and **A1**) have the same reactivity towards the nonchiral MDA substrate. Therefore, there is no point at all in investigating the influence of using different enantiomers of **A1** or **A2** on the polymerization mechanism. For consistency, however, we nonetheless used the correct enantiomer of **A2** as formed upon ligand rotation in **D1** to calculate the next carbene insertion step.
(62) Lamberti, M.; Mazzeo, M.; Pappalardo, D.; Pellecchia, C. *Coord. Chem. Rev.* **2009**, *253*, 2082−2097.
(63) We have thus far not located the transition state **TS5** for rearrangement of **F** to **G**, but it seems unlikely that this process has a high barrier.
(64) Zuidema, E.; Bo, C.; van Leeuwen, P. W. N. M. *J. Am. Chem. Soc.* **2007**, *129*, 3989−4000.
(65) At high MeOH concentrations, proton transfer from the coordinated MeOH moiety to the enolate could also proceed via a hydrogen bonding network chain involving two or more non-coordinated MeOH molecules.[64] However, because the enolate is flexible, such a H-bonding chain is not needed to spatially bridge the distance between the acidic proton and enolate base, and therefore, if any favorable enthalpy effects exist, they are likely small and easily overruled by the unfavorable entropy effects associated with the assembly of such a network. Hence, this possibility was not computationally investigated.
(66) Ahlrichs, R.; Bär, M.; Baron, H.-P.; Bauernschmitt, R.; Böcker, S.; Ehrig, M.; Eichkorn, K.; Elliott, S.; Furche, F.; Haase, F.; Häser, M. ; Hättig, C.; Horn, H. ; Huber, C. ; Huniar, U.; Kattannek, M.; Köhn, A. ; Kölmel, C. ; Kollwitz, M. ; May, K.; Ochsenfeld, H. *Turbomole*, version 6.4; Theoretical Chemistry Group: University of Karlsruhe, 2012.
(67) Treutler, O.; Ahlrichs, R. *J. Chem. Phys.* **1995**, *102*, 346−354.
(68) Schäfer, A.; Horn, H.; Ahlrichs, R. *J. Chem. Phys.* **1992**, *97*, 2571−2577.
(69) Andrae, D.; Haeussermann, U.; Dolg, M.; Stoll, H.; Preuss, H. *Theor. Chim. Acta* **1990**, *77*, 123−141.
(70) *PQS*, version 2.4; Parallel Quantum Solutions: Fayetteville, Arkansas, 2001. (The Baker optimizer is available separately from PQS upon request.)
(71) Baker, J. *J. Comput. Chem.* **1986**, *7*, 385−395.
(72) Budzelaar, P. H. M. *J. Comput. Chem.* **2007**, *28*, 2226−2236.
(73) Lee, C.; Yang, W.; Parr, R. G. *Phys. Rev. B: Condens. Matter Mater. Phys.* **1988**, *37*, 785−789.
(74) Becke, A. D. *J. Chem. Phys.* **1993**, *98*, 5648−5652.
(75) Becke, A. D. *J. Chem. Phys.* **1993**, *98*, 1372−1377.
(76) Calculations were performed using the Turbomole "b3-lyp" functional, which is not completely identical to the Gaussian "B3LYP" functional.
(77) Turbomole Basisset Library, *Turbomole*, version 6.4. D. Andrae, U.; Haeussermann, M.; Dolg, H.; Stoll, H. P. *Theor. Chim. Acta* **1990**, *77*, 123−141.
(78) Schäfer, A.; Huber, C.; Ahlrichs, R. *J. Chem. Phys.* **1994**, *100*, 5829−5835.
(79) Weigend, F.; Häser, M.; Patzelt, H.; Ahlrichs, R. *Chem. Phys. Lett.* **1998**, *294*, 143−152.
(80) Weigend, F.; Ahlrichs, R. *Phys. Chem. Chem. Phys.* **2005**, *7*, 3297−3305.
(81) Grimme, S.; Antony, J.; Ehrlich, S.; Krieg, H. *J. Chem. Phys.* **2010**, *132*, 154104.
(82) Spek, A. L. *PLATON. A Multipurpose Crystallographic Tool*; Utrecht University: Utrecht, The Netherlands, 2003.
(83) Dzik, W. I.; Xu, X.; Zhang, P.; Reek, J. N. H.; de Bruin, B. *J. Am. Chem. Soc.* **2010**, *132*, 10891−10902.
(84) Wertz, D. H. *J. Am. Chem. Soc.* **1980**, *102*, 5316−5322.
(85) Schneider, N.; Finger, M.; Haferkemper, C.; Bellemin-Laponnaz, S.; Hofmann, P.; Gade, L. *Angew. Chem., Int. Ed.* **2009**, *48*, 1609−1613.